

Robust Iris Segmentation Method Based on a New Active Contour Force With a Noncircular Normalization

Mohammed A. M. Abdullah, *Member, IEEE*, Satnam S. Dlay, *Member, IEEE*, Wai L. Woo, *Senior Member, IEEE*, and Jonathon A. Chambers, *Fellow, IEEE*

Abstract—Traditional iris segmentation methods give good results when the iris images are taken under ideal imaging conditions. However, the segmentation accuracy of an iris recognition system significantly influences its performance especially in nonideal iris images. This paper proposes a novel segmentation method for nonideal iris images. Two algorithms are proposed for pupil segmentation in iris images which are captured under visible and near infrared light. Then, a fusion of an expanding and a shrinking active contour is developed for iris segmentation by integrating a new pressure force to the active contour model. Thereafter, a noncircular iris normalization scheme is adopted to effectively unwrap the segmented iris. In addition, a novel method for closed eye detection is proposed. The proposed scheme is robust in finding the exact iris boundary and isolating the eyelids of the iris images. Experimental results on CASIA V4.0, MMU2, UBIRIS V1, and UBIRIS V2 iris databases indicate a high level of accuracy using the proposed technique. Moreover, the comparison results with the state-of-the-art iris segmentation algorithms revealed considerable improvement in segmentation accuracy and recognition performance while being computationally more efficient.

Index Terms—Active contour, biometrics, image segmentation, iris recognition, morphological operations, skin detection.

I. INTRODUCTION

AMONG the various traits used for human identification, the iris pattern has gained an increasing amount of attention for its accuracy, reliability, and noninvasive characteristics. In addition, iris patterns possess a high degree of randomness and uniqueness which is true even between identical

Manuscript received January 5, 2016; accepted April 5, 2016. Portions of the research in this paper use the CASIA-IrisV4 collected by the Chinese Academy of Sciences, Institute of Automation (CASIA). The work of M. A. M. Abdullah was supported by the Ministry of Higher Education and Scientific Research, Iraq. This paper was recommended by Associate Editor S. Agaian.

M. A. M. Abdullah is with the Communications, Sensors, Signal and Information Processing Research Group, School of Electrical and Electronic Engineering, Newcastle University, Newcastle upon Tyne NE1 7RU, U.K., and also with the Department of Computer and Information Engineering, University of Mosul, Mosul 41002, Iraq (e-mail: m.a.m.abdullah@ncl.ac.uk; mabdu@uomosul.edu.iq).

S. S. Dlay, W. L. Woo, and J. A. Chambers are with the Communications, Sensors, Signal and Information Processing Research Group, School of Electrical and Electronic Engineering, Newcastle University, Newcastle upon Tyne NE1 7RU, U.K. (e-mail: satnam.dlay@ncl.ac.uk; lok.woo@ncl.ac.uk; jonathon.chambers@ncl.ac.uk).

Color versions of one or more of the figures in this paper are available online at <http://ieeexplore.ieee.org>.

Digital Object Identifier 10.1109/TSMC.2016.2562500

twins and the iris remains constantly stable throughout an adult's life [1].

Iris segmentation is an essential module in an iris recognition system as the performance of the system is highly dependent on this step and errors can lead to misclassification during authentication. This step involves isolating the iris structure from other components in an eye image, including the pupil, sclera, eyelashes, eyelids, and reflections.

For iris segmentation, several researchers [1]–[4] assume that the inner and outer iris boundaries are circular. This is a source of error, since the pupil boundary is not exactly a circle even in cooperative recognition [5]. In addition, Proenca and Alexandre [6] observed a significant degradation of iris recognition rates, especially in the presence of translation errors of the segmented pupil border. On the other hand, the outer iris boundary appears to be noncircular and nonelliptical in nonideal images such as off-axis iris images. Moreover, simple shape assumptions for iris segmentation are not efficient as the iris is partially deformed by eyelids, eyelashes, and reflections.

All of these challenges explain the importance of using a noncircular approach for iris segmentation. The active contour is an ideal candidate for this purpose [7]. However, there are various drawbacks in the previous active contour models which make them inefficient for a precise iris segmentation. For instance, the snake active contour [8] is sensitive to the initial curve and cannot detect nonconvex objects [9]. Although the problems associated with the snake active contour were alleviated by Xu and Prince [9] in the gradient vector flow (GVF) active contour, the GVF active contour still suffers from the formation of minimum energy points and stopping at spurious edges. In addition, the traditional snake and the GVF models are designed to shrink to reach the target boundary. Therefore, the contour is going to shrink and disappear if the initial mask lies inside of the target object [10].

To solve these drawbacks we propose a new active contour model for iris and image segmentation with robust initialization by integrating a new pressure force within the GVF model which addresses the drawbacks of previous active contour models. The movement direction of the active contour is geared based on the eyelid location. In summary, our contributions are as follows.

- 1) A novel iris segmentation method aiming at improving the recognition performance for iris biometrics both for visible light and near infrared (NIR) imaging.

- 2) A shrinking and expanding active contour integrated with a pressure force to segment the iris accurately.
- 3) A novel method for discarding the images with an invalid iris and limiting the search region in the nonskin parts for irises captured with visible light.

The rest of this paper is organized as follows: in the next section, we present a literature review on iris segmentation; following this we introduce the proposed active contour model. Section IV discusses the iris segmentation and normalization methods in detail. The results are presented and discussed in Section V. Finally, we draw our conclusions in Section VI.

II. RELATED WORK

Many iris segmentation algorithms have been proposed. These algorithms can be broadly classified into three categories of iris segmentation: 1) iris segmentation with the classical circular approaches and their improvements; 2) iris segmentation with noncircular approaches; and 3) iris segmentation with active contour models.

Several traditional iris segmentation algorithms have been suggested including the well-known algorithms proposed by Daugman [1] and Wildes [2]. Daugman [1] used the integro-differential operator (IDO) to find the assumed circular boundaries of the iris. On the other hand, Wildes [2] applied an edge detector followed by a circular Hough transform (CHT) to localize the iris. Later, several others [11]–[13] also proposed iris segmentation methods based on the CHT. Other methods based on the approximation of circular iris boundaries have also been implemented such as the least squares method proposed by Zhu *et al.* [3] and the Hough transform with IDO proposed by Abidin *et al.* [4].

The above classical approaches achieved good performance when the original iris images were captured in ideal conditions. However, there are major drawbacks with these algorithms. For instance, all these methods locate the iris by considering it as a standard circle which causes errors in terms of segmentation. The need for an exhaustive search for circles over a large N^3 parameter space also makes the procedure time consuming [14]. To solve the drawbacks of the previous traditional algorithms, some improved iris segmentation algorithms have been proposed. As a case in point, Tan *et al.* [15] estimate a coarse location of the iris using a clustering algorithm then the iris is segmented with a modified IDO which has lower computation time. Sahmoud and Abuhaiba [16] proposed an iris segmentation algorithm which starts by determining the expected region of the iris using the K -means clustering algorithm to reduce the search region, then the CHT is applied in order to estimate the iris radius and center. Radman *et al.* [17] adopted an improved IDO to segment the iris. In their approach the approximate position of the pupil center is determined using the circular Gabor filter to reduce the search time. Then, the iris and pupil circles are localized using the IDO. Wan *et al.* [18] presented circle-based iris segmentation wherein a Laplace pyramid is incorporated to save computation time. Noise and reflections are removed by anisotropic diffusion and morphological operations, then the innovated curve evolution is used to detect the exterior

boundary. Although the processing time is improved in the aforementioned methods, the application of these algorithms is limited to ideal iris images as they have adopted a circular model assumption.

Later other researchers employed noncircular iris segmentation approaches. For instance, He *et al.* [19] extracted an approximate position for the iris using an AdaBoost-cascade iris detector followed by an elastic model called pulling and pushing for iris segmentation. Zuo and Schmid [20] used ellipse fitting with thresholding for isolating the pupil. As for the limbic boundary, IDO is applied but a heavy computational load is involved. Jan and Usman [21] adopted a twofold scheme based on a circu-differential accumulator and gray statistics to localize a coarse iris region. However, they tested their method on relatively easy iris databases acquired under a controlled environment. More recently, Frucci *et al.* [22] adopted the watershed transformation and circle fitting for iris segmentation. Although a noncircular method is adopted for the outer iris boundary, the pupil is segmented using a circular approach. Unfortunately, this may not provide an accurate segmentation as the pupil appears to be noncircular especially in the nonideal iris images. In addition, they only tested their method on visible light iris images.

Recently, work using an active contour emerged in the literature and several researchers proposed different nonideal iris recognition schemes. For example, Daugman [23] proposed the Fourier active contour approach to model the pupil and the iris boundaries. This method, however, requires good quality iris images with high contrast [23]. Vatsa *et al.* [24] proposed an iris segmentation algorithm that uses a modified energy function and computes the exact iris boundaries by evolving an initial contour in a close region within 5 to 10 pixels. The problem with this algorithm is that the method could not segment the iris if the initial contour was placed far from the actual iris boundaries. Shah and Ross [25] proposed a method to detect the boundary of the iris based on a geodesic active contour. Unfortunately, because the stopping criterion of this method does not take into account the amount of edge detail, the evolving contour might not stop at the desired iris boundaries [25]. Talebi *et al.* [26] used a balloon active contour to segment the iris images from the CASIA version 1.0 database. However, the drawback with this method is that the initial mask for the active contour is set manually.

On the other hand, others [27]–[29] proposed an automated method to estimate the approximate boundaries of the iris then they implemented the active contour to find the accurate pupil and iris boundaries. As a case in point, Roy *et al.* [27] applied direct least squares based elliptical fitting to obtain an initial curve for the active contour. Similarly, Koh *et al.* [28] and Hilal *et al.* [29] took advantage of the CHT to initialize the active contour. Although these methods achieved good results, the main limitation is the complexity of the methods that are used to initialize the active contour compared with the simple approach that we adopt in this paper, and is later explained.

Research in iris segmentation has been gaining more attention in recent years due to the interest in iris recognition at a distance [30]. In addition, competitions such as the mobile iris challenge evaluation [31] focus on the processing of visible

light iris images. This has sparked more work on iris segmentation as the traditional iris segmentation algorithms cannot cope with such imaging [32]–[34]. One of the main aims of this paper is to propose a robust iris segmentation algorithm to address this challenge.

III. ACTIVE CONTOUR MODEL

An active contour is a curve that can move within an image from an initial state into a position where its energy is minimized under the influence of internal forces and image forces that pull it toward features such as lines and edges. These curves are called snakes because of the way the contours move while the energy is minimized. The active contour has become popular in computer vision fields such as edge extraction, image segmentation, motion tracking and 3-D reconstruction [7], [35]. In the next sections, active contour models and the proposed model will be discussed in detail.

A. Active Contour Model

The snake is represented by a curve $v(s) = [x(s), y(s)]$ $s \in [0, 1]$, where s represents the length of the curve. The snake energy is defined as

$$E_{\text{snake}} = \int_0^1 E_{\text{int}}(v(s)) ds + \int_0^1 E_{\text{ext}}(v(s)) ds. \quad (1)$$

The terms $E_{\text{int}}(v(s))$ and $E_{\text{ext}}(v(s))$ represent, respectively, the internal and external energy of the snake. The internal energy is used to control the deformability of the snake, and is written as

$$E_{\text{int}}(v(s)) = \frac{1}{2} (\alpha(s)|v_s(s)|^2 + \beta(s)|v_{ss}(s)|^2) \quad (2)$$

where v_s is the first spatial derivative which represents elasticity, or membrane-like behavior, while the second term v_{ss} is the second spatial derivative and represents rigidity or thin-plate behavior. The coefficients α and β are weighting parameters that control, respectively, the elasticity and rigidity of the contour.

The external energy function is derived from the image energy. For example, in the case where edges of the image are of interest, the energy can be defined as

$$E_{\text{ext}}(v(s)) = -|\nabla(G_\sigma(x, y) * I(x, y))|^2 \quad (3)$$

where $G_\sigma(x, y)$ is a Gaussian function with standard deviation σ , ∇ is the gradient operator, and $*$ represents convolution while $I(x, y)$ is the image intensity function. This convolution smoothes the image to eliminate noise.

Substituting (2) and (3) in (1), gives us the whole expression of the snake

$$E_{\text{snake}} = \int_s (1/2(\alpha(s)|v_s(s)|^2 + \beta(s)|v_{ss}(s)|^2) - (\nabla G_\sigma(x, y) * I(x, y))^2) ds. \quad (4)$$

A snake minimizing (4) must satisfy the following Euler equation [9]:

$$\alpha v_{ss} - \beta v_{ssss} - \nabla E_{\text{ext}} = 0. \quad (5)$$

Solution of the above equation gives the final contour minimizing E_{snake} . This equilibrium function could be considered as the force equilibrium function and is written as

$$F_{\text{int}} + F_{\text{ext}} = 0. \quad (6)$$

The internal force discourages stretching and bending while the external force pulls the snake toward the desired image edges. Therefore, when the original contour evolves and deforms into the final contour ($F_{\text{int}} = -F_{\text{ext}}$) this means that for every point along the curve the internal and external forces are equal and act in opposite directions to each other giving a stable state.

The snake active contour proposed by Kass *et al.* [8] has deficiencies. The two main drawbacks are the sensitivity to the initial curve and failure to detect nonconvex objects [9]. Solution to these problems were provided by Xu and Prince [9] in the GVF active contour which will be discussed in the next section.

B. Gradient Vector Flow Active Contour

The traditional snake model has drawbacks as discussed earlier. Much of the reason for poor performance was attributed to the external force. To ameliorate this problem, Xu and Prince [9] proposed a new snake known as the GVF snake. The basic model for the GVF snake was the same as the traditional snake but with a new external force field ($E_{\text{ext}} = V$) known as the GVF field which was more suitable than the external potential force field and overcame the deficiencies of the previous model.

The GVF snake is defined as a contour $v(s) = (x(s), y(s))$ which satisfies the following Euler equation:

$$\alpha v_{ss} - \beta v_{ssss} - V = 0 \quad (7)$$

where $V(x, y) = (u(x, y), v(x, y))$ is the vector field which substitutes the external vector force field E_{ext} of the traditional snake. The internal forces are defined similar to the original model consisting of elastic and bending forces. The edge map $f(x, y)$ of the image can be defined as follows:

$$f(x, y) = |\nabla(G_\sigma(x, y) * I(x, y))|^2. \quad (8)$$

$V(x, y)$ is then defined to be a vector field which minimizes the following energy functional:

$$\iint \mu(u_x^2 + u_y^2 + v_x^2 + v_y^2) + |\nabla f|^2 |V - \nabla f|^2 dx dy \quad (9)$$

where u_x, u_y, v_x , and v_y are the partial derivatives of $u(x, y)$ and $v(x, y)$ in the x and y directions.

With reference to (9) it can be seen that when the contour is far from the object boundary, ∇f becomes small and the first term of the equation dominates yielding a slowly varying field. On the other hand, when the contour is near the object boundary, ∇f becomes large and the second term dominates. This equation can be minimized by setting $V = \nabla f$. The parameter μ is a regularization parameter governing the tradeoff between the first term and the second term which should be set higher in noisy images. For additional details on the GVF model equations derivation, we refer the reader to [9].

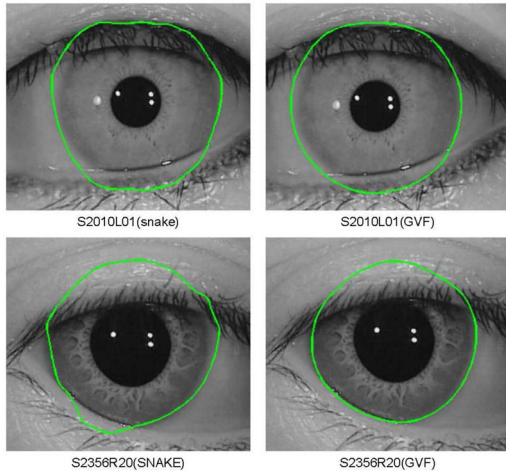


Fig. 1. Segmenting different iris images from the CASIA-IrisV4-Lamp with the traditional snake (left column) and the GVF model (right column). The images are cropped for illustration purpose.

The GVF active contour solved the problems associated with the traditional active contour because the new model is less sensitive to initialization and can detect nonconvex objects. However, the GVF active contour still suffers from the formation of minimum energy points in the case of noisy images and stopping at spurious edges. In addition, the traditional snake model and the GVF model are designed to shrink to reach the target boundary. Therefore, they must be initialized outside the object boundary or else the contour would not reach the object boundary; if it lies inside of the target contour it is going to shrink and disappear [10].

To solve these drawbacks we propose a to integrate a pressure force to the GVF active contour model as described in the next section.

C. Proposed Active Contour Model

It is difficult to segment the outer iris boundary because the iris is often occluded by eyelids or eyelashes and there is low contrast difference between the iris and sclera in some cases. Therefore, methods based on a nonparametric curve such as an active contour are appropriate, however, these methods need to be adapted to achieve an accurate iris segmentation.

Applying the traditional snake active contour will not give good results even if a GVF model is used as the contour will not stop at the desired boundary. This is because both models need to be initialized outside the object boundary in order to converge correctly. Therefore, in the case of an outer iris boundary segmentation, the contour would be trapped at the eyelids and never reach the zone of interest even if the “GVF” model is used as shown in Fig. 1.

In order to handle these problems, a new GVF model with an added pressure force is proposed. Hence, the initial mask of the active contour is set to lie inside the iris boundary (see Section IV-B) and we propose to add another force to the external force of the GVF active contour model. This force acts as a pressure force that pushes the contour to the object boundary. Without this pressure force, even if we have perfect edge detection, the curve will shrink and vanish. Moreover,

this force also solves the problem of contour stopping at the weak edges since it urges the contour to override them.

In this new model, the external force consists of the GVF force and an internal pressure force which acts in a direction normal to the curve to push it outward. So, (7) can be rewritten as follows:

$$\alpha v_{ss} - \beta v_{ssss} - V + K\bar{n}_{(s)} = 0 \quad (10)$$

where $\bar{n}_{(s)}$ is the unit vector normal to the contour at point $v(s)$ and K is the amplitude of this force. The amount of the pressure forces can be controlled by adjusting the value of K .

In some applications a shrinking active contour model is required. This can be achieved by changing the sign of the pressure force in (10) so the new equation can be written as

$$\alpha v_{ss} - \beta v_{ssss} - V - K\bar{n}_{(s)} = 0. \quad (11)$$

A unit normal vector of a curve is perpendicular to the curve at a given point. This means a normal vector of a curve at a given point is perpendicular to the tangent vector at the same point. In summary, a normal vector of a curve is the derivative of the tangent vector of a curve divided by its amplitude as follows:

$$\bar{n}_{(s)} = \frac{T'(s)}{\|T'(s)\|} \quad (12)$$

where $T(s)$ is the unit tangent vector, $T'(s)$ is its derivative, and $\|\cdot\|$ defines the Euclidean norm. This pressure force not only pushes the contour outward, but also it prevents the curve from being trapped by spurious edge points. The proposed active contour model is integrated with the proposed iris segmentation method as explained in the following section.

It can be argued that the proposed pressure force is similar to the adaptive force proposed in [36]. We remark, however, that this force was added to the original snake model which makes it susceptible to well-known snake deficiencies [9]. In addition, the traditional snake and GVF models can only move in one direction (shrink). The proposed model in this paper addresses the aforementioned drawbacks of the previous models and allows the GVF model to move in both directions (expand or shrink) which makes it adequate for various image segmentation applications including iris segmentation.

IV. PROPOSED METHOD

The proposed method in this paper is designed to achieve robust and accurate iris segmentation with high recognition rates for iris images where both pupil and iris appear to be noncircular, and there are several occlusions by eyelashes and eyelids.

The iris segmentation algorithm proposed in this paper has been divided into two main stages. The first stage is on pupil segmentation (in Section IV-A). The second stage is on iris segmentation (in Section IV-B). In order to complete the iris recognition system and evaluate the results of the iris segmentation algorithm, a noncircular iris normalization scheme is discussed in Section IV-C, and finally feature extraction and matching are presented in Section IV-D.

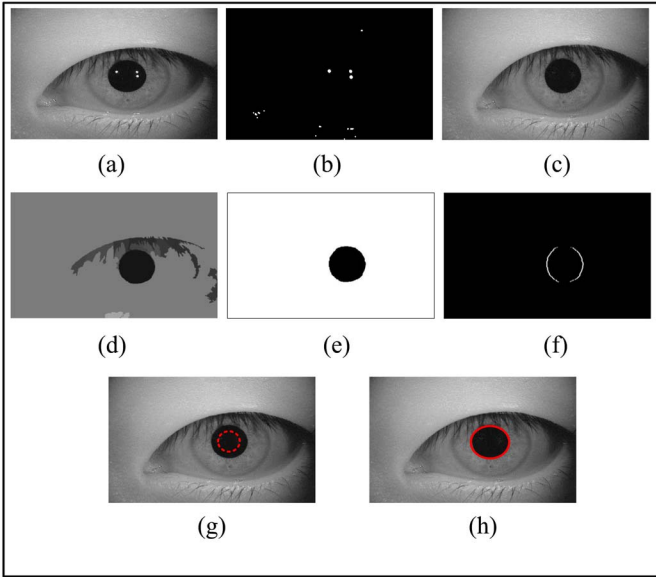


Fig. 2. Steps of the pupillary detection algorithm for the iris images captured under NIR light. (a) Eye captured under NIR light. (b) Reflection map. (c) Inpainted image. (d) Mean shift segmentation. (e) Thresholding and morphological cleaning. (f) Vertical edge map. (g) Set the initial mask of the pupil. (h) Accurate pupil segmentation with the active contour.

A. Pupil Segmentation

We tried to cover all the possible conditions for iris image capturing. Therefore, the experiments in this paper are conducted over two types of iris images: one for iris images which are captured under NIR light and the second for images captured under visible light.

If the iris image is taken under NIR light, the pupil will appear darker than its surrounding with high contrast between the pupil and the iris region [see Fig. 2(a)] [37]. Hence, methods based on thresholding are convenient for isolating the pupil from the rest of the iris image and finding its coarse parameters. However, if the iris images are captured under visible light, the contrast difference between the pupil and the iris is low as shown in Fig. 5(a) so a different approach should be adopted to find the pupil coarse parameters. Accordingly, the proposed pupil segmentation method in this paper can work with two different types of iris images: 1) segmentation of the pupil captured under NIR light and 2) segmentation of the pupil captured under visible light.

1) Segmentation of the Pupil Captured Under NIR Light:

In this section, we propose a fast and accurate method to segment the pupil in iris images captured under NIR light as in the CASIA V4.0 and MMU2 databases. Here we propose to use the mean shift and morphological operations combined with the proposed active contour to segment the pupil accurately. The mean shift is used to cluster the iris image while the morphological operations are used to determine the approximate boundary of the pupil region then the proposed active contour is used to find the precise boundary.

For illustration purposes, Fig. 2 shows the major steps involved in the processing procedures and the obtained results. More specifically, the module broadly consists of the following substeps: 1) reflection removal; 2) mean shift; 3) detecting the

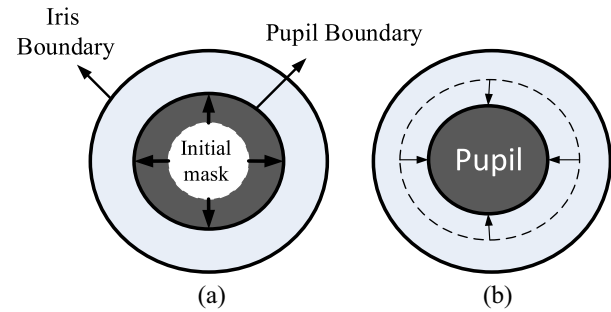


Fig. 3. Initial mask evolving toward the final pupil boundary with the (a) proposed expanding active contour for pupil segmentation in the NIR iris images and the (b) proposed shrinking active contour for pupil segmentation in visible light iris images.

coarse parameters of the pupil; and 4) pupil accurate segmentation with active contour. Detailed description of the signal processing procedures involved in each step are given in the next sections.

a) Reflection removal: The pupil region has some light reflection spots which typically have the highest values in the iris images taken under the NIR light as shown in Fig. 2(a). Local adaptive thresholding is used to build the binary reflection map [Fig. 2(b)] by calculating an individual threshold for each pixel within a window of 30×30 pixels based on the intensity values of the local neighborhood of that pixel. Next, those reflection regions are filled with image inpainting from the nearest neighbors as shown in Fig. 2(c).

b) Mean shift: Mean shift is a nonparametric space analysis technique for determining the maxima of a density function. Mean shift can be widely adjusted to different applications including clustering, image segmentation, and object tracking [38]. We propose to use the mean shift for image clustering which has been applied in this paper with a uniform kernel. The eyelashes are mitigated in the resultant image while large objects such as the pupil are retained as shown in Fig. 2(d). The number of clusters is regulated by the kernel bandwidth parameters (h_s, h_r) as in [38] which are set empirically to be (4, 3) in this paper. In addition, spatial regions containing less than 700 pixels are eliminated to reduce the noise in the resultant image.

c) Detecting the coarse parameters of the pupil: After applying the mean shift, the pupil can be easily isolated by adaptive thresholding based on Otsu's method [39]. Then, a morphological dilation operation with a square structuring element is applied to the binary image in order to eliminate the effect of eyelashes.

Once the pupil is isolated, the CHT can be applied on the resultant binary image to detect the pupil's coarse parameters. After applying the Canny edge detector, only the vertical edges of the pupil are used as an input to the CHT [Fig. 2(f)] in order to reduce the influence of the eyelids. The search region for the CHT will be limited to the pupil part. This will not only reduce the processing time of CHT significantly, but also reduce the errors of the false circle detection by CHT due to the removing of unwanted edges.

d) Pupil accurate segmentation with active contour: The detected pupil parameters from the CHT in the previous substep are used to set the initial mask of the pupil which lies

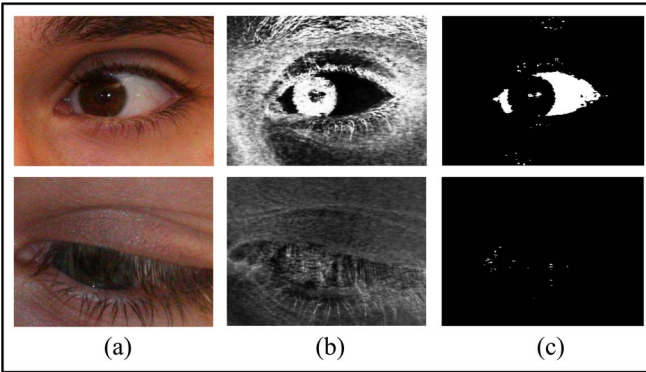


Fig. 4. Sclera detection to discard the closed eye images: the eye image in the bottom row is discarded because the iris and sclera are heavily occluded. (a) Original image. (b) S component of the HIS color space. (c) Thresholded image.

inside the pupillary region as shown in Fig. 3(a). Finally, the pupil's accurate boundary is detected with the proposed active contour. Hence, the previously estimated mask is used as an initial mask for the expanding active contour. This, consequently, will improve the accuracy of the final contour and reduce the number of iterations.

2) Segmentation of the Pupil Captured Under Visible Light: As mentioned earlier, isolating the pupil by thresholding will probably fail when the iris image is captured under visible light because of the low contrast difference between the pupil and the iris especially in dark pigmented iris images. There has been an increasing attention for iris images taken with the visible wavelength under an uncontrolled environment due to different applications such as surveillance [30]. The irises in such images vary in size and location and contain multiple noise factors as in the UBIRIS V1 and UBIRIS V2 databases. Therefore, to segment the pupil and find its coarse parameters we adopted the following approaches. First, a novel method is proposed to discard the images that contain an invalid iris such as in the cases of closed or severely occluded iris based on the sclera presence. Next, after removing the reflection spots, a skin detection method is adopted in order to reduce the search region for the pupil within the nonskin regions. Later, the CHT is applied on the vertical edges of the nonskin regions to find the coarse parameters of the pupil and set the initial mask for the active contour. Finally, the proposed shrinking active contour is applied to segment the pupil accurately. Details of these operations are described in the next sections.

a) Closed eye detection: When the iris images are captured in an uncontrolled environment, it is likely that there are some cases where the eyelids are occluding the iris partially or completely. Therefore, the following method is proposed in order to discard these bad images. Since the sclera is the most easily distinguishable part in the eye image captured under visible light [40], the HSI color model is utilized in sclera isolation. The HSI color model represents every color with three components: 1) hue (H); 2) saturation (S); and 3) intensity (I). The saturation component (S) indicates how much the color is affected by white color. Therefore, this component can be used as an indication for the sclera presence. First, the eye image is converted to the HSI color space then histogram

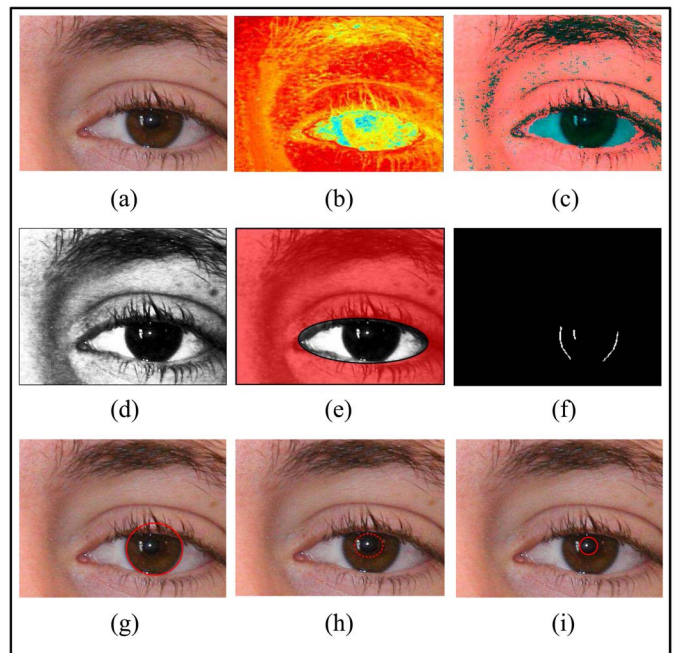


Fig. 5. Steps of the pupillary detection algorithm for the iris images captured under visible light. (a) Eye captured under visible light. (b) Skin likelihood of each pixel. (c) Skin detection. (d) Red chroma of the YCbCr. (e) Nonskin region. (f) Vertical edge map of the nonskin region. (g) CHT. (h) Set the initial mask for the active contour. (i) Pupil accurate segmentation.

equalization is applied to enhance the contrast of the sclera region in the S component of the eye image. Experimental analysis showed that the saturation value in the sclera region varies from 0 to 0.31 so Otsu's adaptive thresholding method is used to select the correct value which separates the sclera in each eye image. After thresholding, if the white pixels count is less than 1000 pixels the eye image is discarded. This value is set empirically because it is noticed that the iris in this case is very small and not usable. Fig. 4 illustrates the proposed closed eye detection method. While the first row of this figure shows a valid eye image with good pixels count in the thresholded S component, the second row shows a heavily occluded eye image which has been discarded due to the limited pixels count in the resultant thresholded image. It should be noted that this method can be used efficiently to detect the presence of the sclera in an eye image, nevertheless, it may not provide an accurate segmentation for the sclera in all the cases.

b) Skin detection: We propose to use a skin detector model to limit the search for the pupil in the nonskin regions only. The discrimination between the skin and nonskin pixels is carried out by introducing a skin color model which calculates the distance of the pixel color to skin color. Following the works of [41] and [42], a nonparametric skin model is created using manually annotated skin and nonskin pixels. The pre-trained model for skin detection accommodated 138 571 957 pixels in total. The former model is used to estimate the skin color distribution without deriving an explicit model. Next, a Bayes' classifier is used to calculate the skin probability of each pixel [Fig. 5(b)] and the skin likelihood image is computed with respect to the trained data. Finally, this likelihood image is thresholded at the zero level to generate the skin map



Fig. 6. Attenuation of eyelashes with 2-D order-statistic filter. Left column shows the original iris images while the right column shows the processed images.

as shown in Fig. 5(c) and morphological image closing is used to close the small gaps in the resultant skin map.

c) Detecting the coarse parameters of the pupil: The YCbCr color space is utilized because it is capable of maximizing the contrast between the sclera and iris [40]. The histogram equalization is applied to the original image then the red chroma component of the YCbCr color space is extracted and the histogram equalization is applied again [Fig. 5(d)]. Next, the Canny vertical edge detector is applied on the non-skin regions as illustrated in Fig. 5(e) and (f). Later, the CHT is applied to the resultant edge image to determine the coarse pupil parameters.

d) Pupil accurate segmentation with active contour: The circle parameters obtained from the previous step are used to initialize the active contour. Accordingly, the center of the initial mask is set to be the same center of the iris obtained from the previous step. Although the pupil and iris centers are known to be nonconcentric, this small translation of the initial mask will not affect the active contour convergence.

On the other hand, for calculating the radius of the initial mask [Fig. 5(h)], the iris radius obtained previously from the CHT is utilized. From physiology, the ratio between the radii of the iris and the pupil is approximately 3 : 1 [43]. Hence, the radius of the initial circle is set to be 2/3 of the iris radius to make sure that the initial circle always lies outside the pupil boundary even under low illumination conditions when the pupil becomes dilated. Then the proposed shrinking active contour model [Fig. 3(b)] is employed to segment the pupil accurately as shown in Fig. 5(i).

B. Iris Segmentation With the Proposed Active Contour

Segmenting the outer iris boundary is a challenging task as the contrast difference between the pupil/iris or iris/sclera is not very high. Moreover, the appearance of eyelids and eyelashes hinders the segmentation process. Therefore, a robust segmentation method should be designed to achieve an accurate iris segmentation. The proposed iris outer borderer segmentation algorithm consists of the following steps.

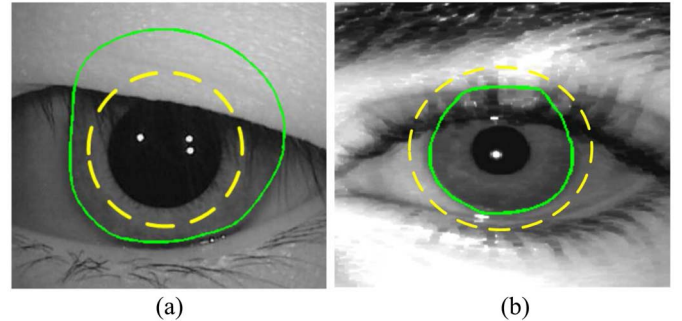


Fig. 7. Unsuccessful iris segmentation with the (a) expanding active contour and the (b) shrinking active contour.

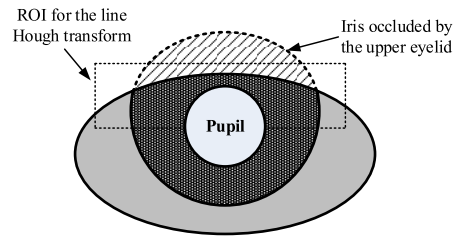


Fig. 8. Utilizing the line Hough transform to check the occlusion by the upper eyelid to determine whether to use the proposed shrinking or expanding active contour.

1) Eyelashes Removal: Eyelashes need to be removed before applying the active contour to detect the iris boundary as they affect the contour convergence. To cure this problem, 2-D order-statistic filtering is applied on the iris images. Our experiments indicate that setting the size of the window to $[2 \times 10]$ with an order of 16 removes most of the eyelashes as shown in Fig. 6. The remaining eyelashes are either eliminated or weakened so the proposed active contour model is able to pass them due to the added pressure force.

2) Active Contour Initialization: After the pupil has been segmented, the active contour is initialized by a new circular mask which is created outside the pupil. The radius of this new mask is set to be larger than the radius of the final contour obtained from the segmentation of the pupil. This ensures the initial curve lies outside the pupil boundary in order to converge easily to the iris borderer.

The initial contour is evolved using the proposed active contour model from the initial mask until the energy function is minimized when the curve is on the iris boundary. This grants good segmentation if the eyelids are far from the pupil. However, there are some cases where the upper eyelid is near or covering the pupil; applying the active contour with an initial curve lying outside the pupil for such images will result in the contour bulging outward toward the eyelids as shown in Fig. 7(a). This problem cannot be solved by using only the shrinking active contour because the contour will be trapped at the eyelashes and the fold of the eyelid as shown in Fig. 7(b) which causes false segmentation.

3) Utilizing the Eyelid Position: To deal with this issue, we propose a novel approach. A line Hough transform is applied to the upper portion of the iris image to detect the upper eyelid as shown in Fig. 8. Hence, if a line is found in the region of

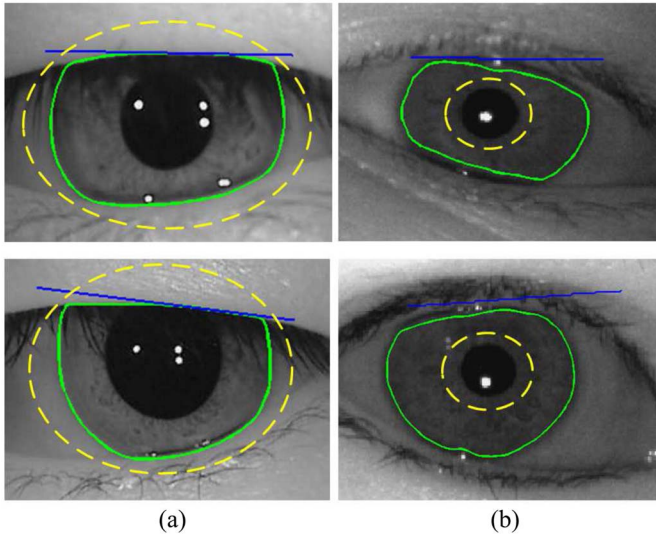


Fig. 9. Initial mask moving toward the final iris boundary, where the blue line represents the detection of the upper eyelid by the line Hough transform and the dotted yellow line represents the initial mask in the (a) shrinking active contour and the (b) expanding active contour.

the initial contour, then the proposed shrinking active contour in (11) is applied.

In this case, the initial mask for the active contour is set to be larger than the iris radius so it can converge correctly to the final contour shown in Fig. 9(a). On the contrary, if the eyelids are not close to the pupil, then the expanding active contour is evolved from the initial mask which lies within the iris as depicted in Fig. 9(b).

4) Eyelids Removal: This approach has the advantage that no separation algorithm is needed in finding the eyelids. Once the contour has converged to its final state, the last estimates of the iris boundaries can be used for removing the eyelids.

C. Noncircular Normalization

Once the segmentation is complete, the next stage is iris normalization. This stage is essential because the size of iris varies from person to person; even for the same person it can change, due to variation in illumination, pupil size and standoff distance. The normalization process involves unwrapping the iris and converting it into the dimensionless polar coordinates as proposed by Daugman [1]. However, the classical normalization approach requires both iris and pupil to be circular in shape and share the same reference point for iris unwrapping. Since the pupil and the iris can be nonconcentric, a remapping formula is proposed by Masek and Kovesi [12] to rescale the centers. Nevertheless, when using noncircular approaches for iris segmentation, iris boundaries could be any kind of curve and finding a reference point becomes difficult so the traditional iris normalization method is inadequate.

Here, we adopted the noncircular iris normalization method from [44]. Instead of representing the iris and the pupil by circles and finding a reference point, the boundaries obtained by the active contour are used directly for this purpose regardless of the iris or pupil centers. Hence, radial lines pass from the

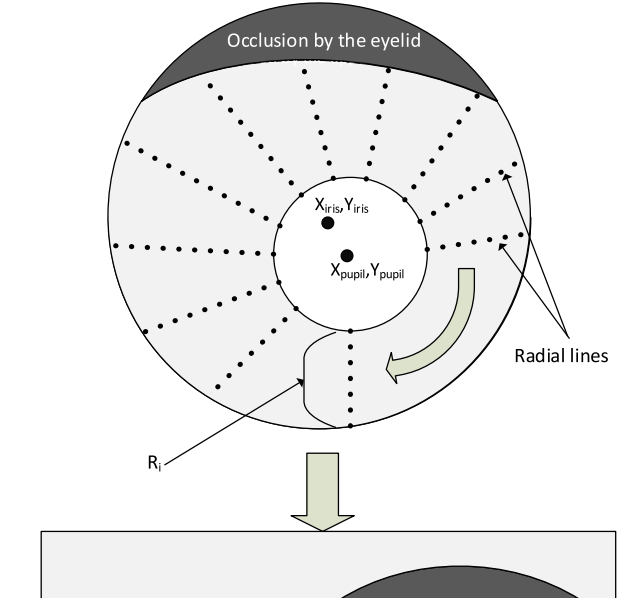


Fig. 10. Diagrammatic of the noncircular normalization method for an off-axis iris image.

pupil contour to the iris contour and are traced back to the pupil center ($X_{\text{pupil}}, Y_{\text{pupil}}$) as shown in Fig. 10. This center represents a point that the pupil center reaches when the pupil radius becomes zero. After that, a number of data points are selected along each radial line.

The length of each radial line is calculated as the distance between the two contours (pupil border to iris border) which can be found as follows:

$$R_i = \sqrt{(x_i - x_p)^2 + (y_i - y_p)^2} \quad (13)$$

where x_i, y_i and x_p, y_p correspond to the iris and pupil contours, respectively. Experiments indicate that choosing 350 radial lines with 50 points in each gives the best result.

This normalization method can be used with any iris segmentation approach and the efficiency of noncircular normalization method can be seen from the improvement of the equal error rate (EER) compared to the traditional circular normalization method as will be illustrated in Fig. 14 and Table III.

It is worth mentioning that although some researchers [25], [26], [45] used active contour models for iris segmentation, for iris normalizing, a traditional circular method was employed. Consequently, this reduced the efficiency of their segmentation methods.

D. Feature Extraction and Matching

Feature encoding is implemented by convolving the normalized iris template with a 1-D log-Gabor filter [12]. Only the phase information is used to encode the iris pattern, because of its robustness to illumination, imaging contrast and camera gain [1]. The output of filtering is then phase quantized to four levels using the Daugman method [1], with each filter producing two bits of data for each phase. At the matching stage, the

Hamming distance has been applied as a metric for recognition. The Hamming distance algorithm also incorporates noise masking so that only significant bits are used in calculating the Hamming distance between two iris templates. The normalization, feature extraction and matching are adopted from the iris recognition system in [12].

V. RESULTS AND DISCUSSION

Experiments were conducted on four iris databases namely: 1) CASIA-IrisV4-Lamp; 2) MMU2; 3) UBIRIS V1; and 4) UBIRIS V2. Most of the images in these databases are challenging and captured under different conditions from a wide variety of ethnicity.

The CASIA-IrisV4-Lamp was released by the Institute of Automation, Chinese Academy of Sciences [46]. It contains 16 212 images from 819 classes. It was collected in an indoor environment with nonlinear deformation due to variations in visible illumination. In addition, it contains many images with heavy occlusion and poor contrast.

The MMU iris databases were provided by the Malaysian Multimedia University in two versions MMU1 and MMU2. The MMU2 iris database [47] consists of 995 iris images which have been collected with distance of 47–53 cm away from the user. Unlike MMU1 which contains a smaller number of samples with few noise factors, the captured iris images in MMU2 contains severe obstructions by eyelids/eyelashes, specular reflection, nonlinear deformation, low contrast, and illumination changes.

On the other hand, the UBIRIS V1 iris image database was released by the University of Beira, Portugal [48]. It contains 1877 images from 241 subjects in two different sessions. All images are taken under visible light. Several realistic noise factors were introduced to the session 2 of the UBIRIS V1 database such as reflections, defocus and oblique views to simulate noncooperative conditions.

Finally, the UBIRIS V2 iris image database was also released by the University of Beira [30]. These images were captured under visible light in unconstrained conditions with more realistic noise factors. In addition, the images were captured on the move with a standoff distance of 4–8 m. The database has 11 102 images in total taken from 261 subjects. A subset of this database that consists of 2250 images from 50 subjects was employed in the experiments because the ground truth of these images are available from the work of Hofbauer *et al.* [32] so the segmentation performance can be measured accurately. Forty images were discarded by the proposed close eye detection method because the iris in these images is either occluded severely or completely. We wish to emphasize that the NICE.I iris segmentation competition was based on only 500 images taken from the UBIRIS V2 database [49]. Therefore, this paper exploits about four and half times the number of the iris images used in the NICE.I competition.

To evaluate the proposed segmentation algorithm, we tested it through segmentation accuracy, recognition performance, computational time and moreover, it is compared with different iris segmentation algorithms in the literature.

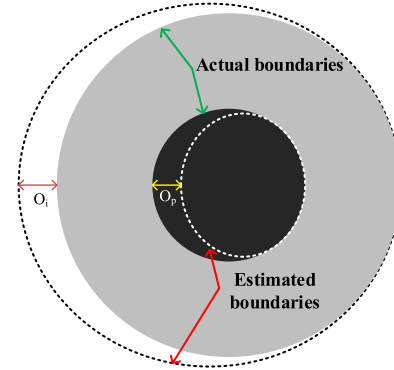


Fig. 11. Visual evaluation criteria.

TABLE I
VISUAL SEGMENTATION RESULTS OF THE IMAGES IN THE
CASIA V4, MMU2, AND UBIRIS V1 DATABASES

Database	Correct	Fair	Bad
CASIA-IrisV4-Lamp	95.1%	2.9%	2%
UBIRIS V1 Session 1	96.5%	2.2%	1.3%
UBIRIS V1 Session 2	94.4%	3.3%	2.3%
MMU2	93.7%	4.1%	2.2%

A. Segmentation Evaluation

The evaluation of iris segmentation results is a challenging issue because the ground truth is not available for all the images. Therefore, visual inspection is used to judge the performance where the ground truth is not available for the iris databases of CASIA V4, MMU2, and UBIRIS V1. On the other hand, the ground truth for 2250 images from the UBIRIS V2 was made available by the work of Hofbauer *et al.* [32]. A mathematical model was used to measure the segmentation performance as illustrated later in this section. In addition, the overall performance of the biometric system was measured with the receiver operation characteristic (ROC) curves and the EER as illustrated later in Section V-B.

Since the visual inspection is subjective, and different annotators give various results, we adopted, as a measure of visual evaluation, the maximum offset from the pupil boundary O_p and the maximum offset from the iris boundary O_i as shown in Fig. 11. Thus, the segmentation results are divided into three groups correct, fair, and bad.

- 1) *Correct*: The maximum offset between final contour and the actual iris or pupil boundary is no more than three pixels.
- 2) *Fair*: $3 < O_i \text{ and } O_p \leq 10$ pixels.
- 3) *Bad*: $O_i \text{ and } O_p > 10$ pixels.

After applying the proposed method to the iris images, the segmentation results are considered “correct” if the final contour falls on the actual iris and pupil boundaries. On the other hand, “fair” segmentation is achieved when the maximum offset between the real boundary and the final contour boundary is within 3–10 pixels. Anything other than that is treated as “bad.” Fig. 12 shows examples of different segmentation results. The iris segmentation results with the proposed method using the visual inspection are depicted in Table I.



Fig. 12. Segmentation classification results from the CASIA V4, MMU2, and UBIRIS V1 databases. (a) Correct. (b) Fair. (c) Bad.

According to Table I, the highest and lowest percentage of correct segmentation are, respectively, recorded with the UBIRIS V1 session 1 and MMU2 databases. This is because most of the iris images in the MMU2 database contain severe obstructions by the eyelids/eyelashes, specular reflection and blurred iris region. On the contrary, unlike session 2 of the UBIRIS V1 database, the iris region in session 1 of the same database are not occluded severely by the eyelids or blurred.

On the other hand, since the ground truth for the UBIRIS V2 database is available, a mathematical method based on the total number of the disagreeing pixels between the segmented image mask and its ground truth is adopted. Let I_i be the input image, $O(c', r')$ the output image segmentation mask and $C(c', r')$ is its ground-truth. All the images of I_i , O and C have the same dimensions. Hence, the classification error rate (E_i) can be calculated as the proportion of correspondent disagreeing pixels between the output image and its ground truth as follows [49]:

$$E_i = \frac{1}{c \times r} \sum_{c'} \sum_{r'} O(c', r') \oplus C(c', r') \quad (14)$$

where c' and r' are the pixels of the output image and its ground truth; r and c are, respectively, the number of rows



Fig. 13. Iris segmentation results for images from the UBIRIS V2 database using the proposed method.

and columns of the image while \oplus is the logical XOR operator. The total classification error (E_1) is given by the average of all the errors (E_i)

$$E_1 = \frac{1}{n} \sum_i E_i \quad (15)$$

where n is the total number of images. The total classification error (E_1) for the subset of the UBIRIS V2 database segmented with the proposed method is 2.95%. Examples of these segmentation results are shown in Fig. 13. Table II shows the efficiency of the proposed method compared to others. It can be clearly seen that the proposed iris segmentation method outperforms state-of-the-art methods in terms of the total classification error and processing time.

For the outer iris boundary, the proposed active contour with prior contour initialization converges easily with average number of 75 iterations. As for the inner boundary, only 25 iterations are needed. This is because the initial contour is set to be very close to the actual pupil's shape. For iris segmentation, extensive experiments have been performed to determine a common set of parameters that can be used for accurate iris extraction. Accordingly, the values of these parameters to be used in (10) and (11) are $\alpha = 0.4$, $\beta = 0.2$, and $K = 0.3$. Using these values accurate segmentation results were sustained for iris images.

B. Performance Comparison

In order to evaluate the efficiency of our method, we compared it with the previously quoted techniques in terms of recognition performance and processing time for the CASIA V4, MMU2, and UBIRIS V1 databases. As for the UBIRIS V2 database, we compare the proposed algorithm performance with the reported results in the works of [50], [51], [52], and [53] in terms of the total classification error (E_1) and the processing time. This set of iris images and their respective ground truths are available from the works of Hofbauer *et al.* [32] and Proen  a and Alexandre [49]. For the CASIA V4, MMU2, and UBIRIS V1 databases, the iris segmentation algorithms proposed [9], [25], [26], [54]–[56]¹

¹The source code of the active contour models used to replicate these works is available: <http://uk.mathworks.com/matlabcentral/fileexchange/28149-snake-active-contour/content/Snake2D.m>; <http://uk.mathworks.com/matlabcentral/fileexchange/24998-2d-3d-image-segmentation-toolbox>.

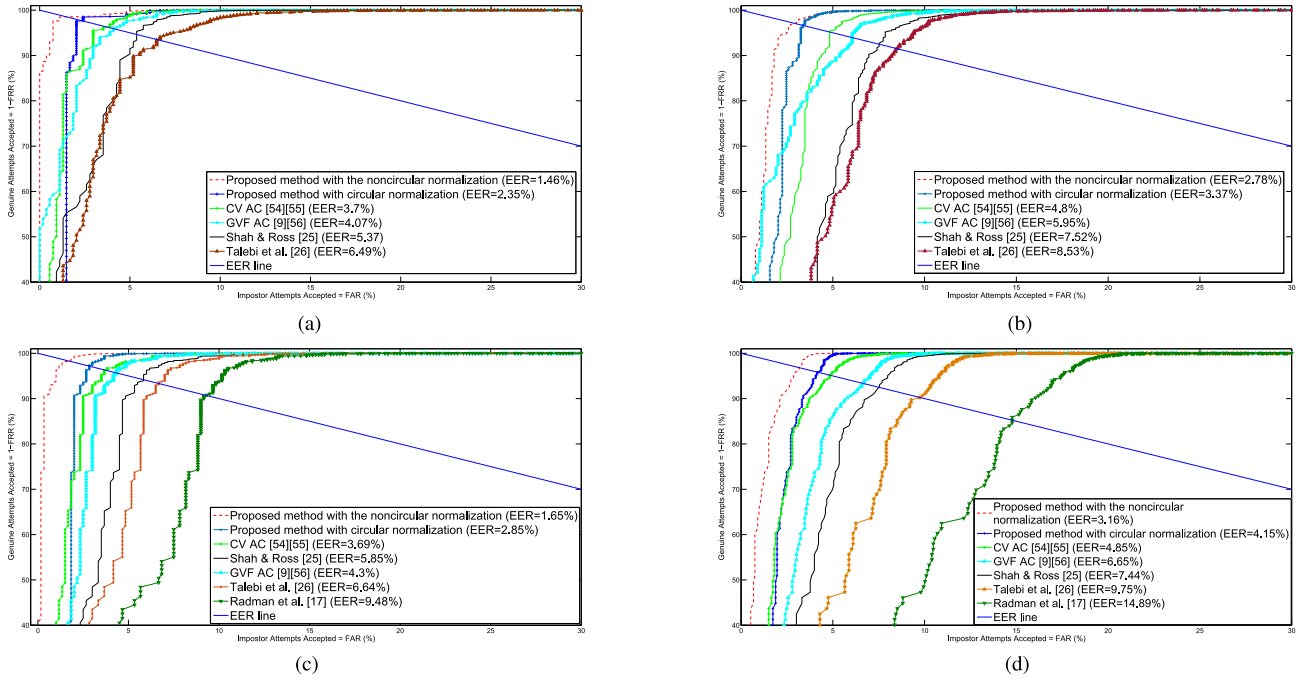


Fig. 14. ROC curves and EERs illustrate the recognition performance of different iris segmentation methods. (a) CASIA-LAMP V4 database. (b) MMU2 database. (c) UBIRIS V1 session 1. (d) UBIRIS V1 session 2.

TABLE II
AVERAGE COMPUTATION TIMES AND THE E_1 ERROR REPORTED
WITH DIFFERENT SEGMENTATION METHODS FOR THE
UBIRIS V2 DATABASE

	Total classification error (E_1)	Time (sec)
Proposed algorithm	2.95%	0.5
Luengo-Oroz et al. [50]	3.05%	3.5
Chen et al. [51]	2.97%	6.77
Labati et al. [52]	3.01%	120
Tan et al. [53]	2.05%	130

are reimplemented and compared with our algorithm through recognition performance. Only the segmentation approaches in the previously stated algorithms are implemented, and then the iris images are processed with the same normalization, encoding and matching procedures presented in this paper. Furthermore, to evaluate the recognition performance, an ROC curve of the proposed algorithm is plotted and the EER is obtained from the ROC curve. Intuitively, the more accurate the segmentation, the higher the recognition performance.

Fig. 14 and Table III illustrate the performance of the proposed algorithm against the performance of the previously stated algorithms [9], [25], [26], [54]–[56] on the images in the CASIA V4, MMU2, and UBIRIS V1 databases. It can be seen from Fig. 14 and Table III that the proposed algorithm achieves the lowest EER. The classical circular approaches for iris segmentation fail in terms of detecting the iris in the nonideal iris images especially under the presence of noise or occlusion. In addition, the circular segmentation methods locate the iris considering it as a standard circle which causes errors in segmentation when the iris appears to be noncircular in nonideal conditions. In our opinion, the high EER reported in [17] is also the result of adopting a circular approach (IDO) for iris segmentation.

TABLE III
PERFORMANCE COMPARISON OF THE PROPOSED METHOD
ON THE IMAGES FROM DIFFERENT DATABASES

Method	CASIA V4	MMU2	UBIRIS V1	
			Session 1	Session 2
Proposed with the noncircular normalization	1.46%	2.78%	1.65%	3.16%
Proposed with circular normalization	2.35%	3.37%	2.85%	4.15%
Shah and Ross [25]	5.37%	7.52%	5.82%	7.44%
Talebi et al. [26]	6.49%	8.53%	6.64%	9.75%
Chan-Vese AC [54], [55]	3.70%	4.80%	3.69%	4.85%
GVF AC [9], [56]	4.07%	5.95%	4.30%	6.65%
Radman et al. [17]	-	-	9.48%	14.89%

Moreover, the recognition performance of our method is better than the other methods based on classical active contour models [9], [25], [26], [54]–[56]. Several aspects contribute to this. First, the coarse iris parameter estimations allow accurate mask initialization for the active contour and hence reduce the convergence time. Second, the integration of the pressure force with the active contour yields an effective curve evolving mechanism. Third, introducing the shrinking and expanding active contour contributes to more efficient iris segmentation for iris images with eyelids which lie close to the pupil. Fourth, adopting noncircular normalization has effectively normalized the segmented portion of the iris. All of these points have resulted in a more accurate and robust iris segmentation and, hence, higher recognition ratio.

On the other hand, the efficiency of the noncircular normalization method can be seen from Fig. 14 and Table III. The achieved improvements in the EER by the this normalization method on CASIA V4, MMU2, UBIRIS V1 session 1, and UBIRISV1 session 2 are 37.87%, 17.5%, 42.1%, and 23.85%, respectively.

As for the UBIRIS V2 database, Table II confirms that the proposed method is superior to the works

TABLE IV
AVERAGE COMPUTATION TIMES (IN SECONDS) OF EACH STAGE
IN THE PROPOSED SEGMENTATION ALGORITHM

	CASIA V4	MMU2	UBIRIS V1	UBIRIS V2
Pupil segmentation	0.32	0.28	0.4	0.24
Eyelid localization	0.01	0.01	0.02	0.01
Iris segmentation	0.31	0.23	0.35	0.25
Total average time	0.65	0.52	0.77	0.5

TABLE V
COMPARISON AMONG THE AVERAGE COMPUTATION TIMES (IN
SECONDS) FOR DIFFERENT IRIS SEGMENTATION METHODS

	CASIA V4	MMU2	UBIRIS V1
Proposed algorithm	0.65	0.52	0.77
Radman et al. [17]	-	-	1.09
Shah and Ross [25]	5.1	4.2	6.2
Talebi et al. [26]	1.8	1.2	2.2
Hilal et al. [29]	4.8	3.9	5.8

of [50], [51], and [52] in terms of the total classification error (E_1) and the computation times.

The smaller classification error reported in [53] can be attributed to the smaller number of iris images employed in their experiment compared to this paper. In addition, significant amount of time is required to complete their segmentation procedure whereas our proposed method achieved improvement of 96.6% in terms of the segmentation time.

C. Computation Time

All experiments were conducted on a 3.2 GHz core i5 processor with 8 GB of RAM under the MATLAB environment. In addition, the time consuming stages such as the CHT are implemented under a C++ environment which is then called by MATLAB with the help of an MEX-file in order to reduce the running time. As for the works of [50]–[53] the experiments were conducted on a 2.2-GHz Intel processor with 2 GB of RAM to achieve a similar environment to the aforementioned works.

The proposed iris segmentation method can be divided into three main stages: 1) pupil segmentation; 2) eyelid detection; and 3) iris-limbic segmentation. Table IV shows the average computation time for each stage of the proposed algorithm which is obtained from averaging the times of the segmentation process of 100 images taken from each database. The variations in the computation times among databases are due to the different images size.

Tables V and II illustrate the average times of different iris segmentation algorithms. As mentioned before, the circle detection approaches are the most time consuming process especially if they are applied directly on the whole image without modification. The long computation time in the Shah and Ross [25] method can be attributed to the circle fitting method used for pupil localization before the active contour is applied. Similarly, Hilal *et al.* [29] applied the CHT to set the initial mask of the active contour. On the other hand, Talebi *et al.* [26] achieved lower time than the previous two methods because no circle fitting is used in their method however, the initial mask of the active contour is set manually. The significant computation time in the Tan and Kumar [53]

method can be attributed to the calculation of the localized Zernike features for every single pixel in the iris image [57].

The proposed method is superior in terms of the computation time of the previous iris segmentation methods [17], [25], [26], [29], [50]–[53] and segmented the iris in less than a second which implies that it is suitable for real time applications.

VI. CONCLUSION

In this paper, a novel method for iris segmentation has been proposed. A new pressure force was designed and integrated with the GVF active contour to allow the contour to expand or shrink, which in turn helps to achieve robust iris segmentation. The proposed iris segmentation process consists of two models: pupil segmentation and iris segmentation. For pupil segmentation, two schemes were proposed to determine the approximate parameters of the pupil in the iris images which are captured under visible and NIR light. These parameters were then used to set the initial mask for the active contour. Initializing the active contour near the desired object boundary helps not only to reduce the execution time by minimizing the number of iterations, but also achieves robust segmentation as the search region is limited by the desired object. On the other hand, for iris segmentation, the line Hough transform was employed for eyelid detection. Hence, if the eyelid is closed or covering the pupil, the contour will shrink from the initial mask which is set to be larger than the iris. In contrast, if the eyelid is not close to the pupil, the contour will expand from the initial mask which is set outside the pupil boundary. The proposed scheme is robust in finding the exact iris boundary and isolating the eyelids of the iris images. Moreover, noncircular iris normalization helped to effectively unwrap the segmented iris. Therefore, instead of representing the iris and the pupil in terms of circles, the obtained boundaries from the active contour are used.

The experimental results on the CASIA V4, MMU2, UBIRIS V1, and UBIRIS V 2 databases showed that the proposed scheme achieves state-of-the-art iris results in terms of segmentation accuracy and recognition performance while being computationally more efficient.

REFERENCES

- [1] J. G. Daugman, "High confidence visual recognition of persons by a test of statistical independence," *IEEE Trans. Pattern Anal. Mach. Intell.*, vol. 15, no. 11, pp. 1148–1161, Nov. 1993.
- [2] R. P. Wildes, "Iris recognition: An emerging biometric technology," *Proc. IEEE*, vol. 85, no. 9, pp. 1348–1363, Sep. 1997.
- [3] Y. Zhu, T. Tan, and Y. Wang, "Biometric personal identification based on iris patterns," in *Proc. 15th Int. Conf. Pattern Recognit.*, vol. 2. Barcelona, Spain, 2000, pp. 801–804.
- [4] Z. Z. Abidin, M. Manaf, and A. S. Shibghatullah, "Iris segmentation analysis using integro-differential and hough transform in biometric system," *J. Telecommun. Electron. Comput. Eng.*, vol. 4, no. 2, pp. 41–48, 2012.
- [5] J. Huang, X. You, Y. Y. Tang, L. Du, and Y. Yuan, "A novel iris segmentation using radial-suppression edge detection," *Signal Process.*, vol. 89, no. 12, pp. 2630–2643, 2009.
- [6] H. Proenca and L. A. Alexandre, "A method for the identification of inaccuracies in pupil segmentation," in *Proc. 1st Int. Conf. Availability Rel. Security. (ARES)*, Vienna, Austria, 2006, pp. 1–5.
- [7] M. Haidekker, *Deformable Models and Active Contours*. Canada: Wiley, 2011, pp. 173–210.

- [8] M. Kass, A. Witkin, and D. Terzopoulos, "Snakes: Active contour models," *Int. J. Comput. Vis.*, vol. 1, no. 4, pp. 321–331, 1988.
- [9] C. Xu and J. L. Prince, "Snakes, shapes, and gradient vector flow," *IEEE Trans. Image Process.*, vol. 7, no. 3, pp. 359–369, Mar. 1998.
- [10] L. D. Cohen and I. Cohen, "Finite-element methods for active contour models and balloons for 2-D and 3-D images," *IEEE Trans. Pattern Anal. Mach. Intell.*, vol. 15, no. 11, pp. 1131–1147, Nov. 1993.
- [11] M. Li, Y. Wang, and T. Tan, "Iris recognition using circular symmetric filters," in *Proc. 16th Int. Conf. Pattern Recognit.*, vol. 2. Quebec City, QC, Canada, 2002, pp. 414–417.
- [12] L. Masek and P. Kovesi, "MATLAB source code for a biometric identification system based on iris patterns," School Comput. Sci. Softw. Eng., Univ. Western Australia, Crawley, WA, Australia, 2003. Accessed on Apr. 2016. [Online]. Available: <http://www.peterkovesi.com/studentprojects/libor/sourcecode.html>
- [13] L. Ma, T. Tan, Y. Wang, and D. Zhang, "Efficient iris recognition by characterizing key local variations," *IEEE Trans. Image Process.*, vol. 13, no. 6, pp. 739–750, Jun. 2004.
- [14] C. Hollitt, "Reduction of computational complexity of Hough transforms using a convolution approach," in *Proc. 24th Int. Conf. Image Vis. Comput.*, Wellington, New Zealand, 2009, pp. 373–378.
- [15] T. Tan, Z. He, and Z. Sun, "Efficient and robust segmentation of noisy iris images for non-cooperative iris recognition," *Image Vis. Comput.*, vol. 28, no. 2, pp. 223–230, 2010.
- [16] S. A. Sahmoud and I. S. Abuhaiba, "Efficient iris segmentation method in unconstrained environments," *Pattern Recognit.*, vol. 46, no. 12, pp. 3174–3185, 2013.
- [17] A. Radman, K. Jumari, and N. Zainal, "Fast and reliable iris segmentation algorithm," *IET Image Process.*, vol. 7, no. 1, pp. 42–49, Feb. 2013.
- [18] H.-L. Wan, Z.-C. Li, J.-P. Qiao, and B.-S. Li, "Non-ideal iris segmentation using anisotropic diffusion," *IET Image Process.*, vol. 7, no. 2, pp. 111–120, Mar. 2013.
- [19] Z. He, T. Tan, Z. Sun, and X. Qiu, "Toward accurate and fast iris segmentation for iris biometrics," *IEEE Trans. Pattern Anal. Mach. Intell.*, vol. 31, no. 9, pp. 1670–1684, Sep. 2009.
- [20] J. Zuo and N. A. Schmid, "On a methodology for robust segmentation of nonideal iris images," *IEEE Trans. Syst., Man, Cybern. B, Cybern.*, vol. 40, no. 3, pp. 703–718, Jun. 2010.
- [21] F. Jan and I. Usman, "Iris segmentation for visible wavelength and near infrared eye images," *Optik Int. J. Light Electron Optics*, vol. 125, no. 16, pp. 4274–4282, 2014.
- [22] M. Frucci, M. Nappi, D. Riccio, and G. Sanniti di Baja, "WIRE: Watershed based iris recognition," *Pattern Recognit.*, vol. 52, pp. 148–159, Apr. 2016.
- [23] J. Daugman, "New methods in iris recognition," *IEEE Trans. Syst., Man, Cybern. B, Cybern.*, vol. 37, no. 5, pp. 1167–1175, Oct. 2007.
- [24] M. Vatsa, R. Singh, and A. Noore, "Improving iris recognition performance using segmentation, quality enhancement, match score fusion, and indexing," *IEEE Trans. Syst., Man, Cybern. B, Cybern.*, vol. 38, no. 4, pp. 1021–1035, Aug. 2008.
- [25] S. Shah and A. Ross, "Iris segmentation using geodesic active contours," *IEEE Trans. Inf. Forensics Security*, vol. 4, no. 4, pp. 824–836, Dec. 2009.
- [26] S. M. Talebi, A. Ayatollahi, and S. M. S. Moosavi, "A novel iris segmentation method based on balloon active contour," in *Proc. 6th Iranian Mach. Vis. Image Process.*, Isfahan, Iran, 2010, pp. 1–5.
- [27] K. Roy, P. Bhattacharya, and C.Y. Suen, "Unideal iris segmentation using region-based active contour model," in *Proc. 7th Int. Conf. Image Anal. Recognit. (ICIAR)*, vol. 6112. Heidelberg, Germany, 2010, pp. 256–265.
- [28] J. Koh, V. Govindaraju, and V. Chaudhary, "A robust iris localization method using an active contour model and Hough transform," in *Proc. 20th Int. Conf. Pattern Recognit. (ICPR)*, Istanbul, Turkey, 2010, pp. 2852–2856.
- [29] L. Hilal, B. Daya, and P. Beausery, "Hough transform and active contour for enhanced iris segmentation," *Int. J. Comput. Sci. Issues*, vol. 9, no. 6, pp. 1–10, 2012.
- [30] H. Proenca, S. Filipe, R. Santos, J. Oliveira, and L. A. Alexandre, "The UBIRIS.v2: A database of visible wavelength iris images captured on-the-move and at-a-distance," *IEEE Trans. Pattern Anal. Mach. Intell.*, vol. 32, no. 8, pp. 1529–1535, Aug. 2010.
- [31] M. De Marsico, M. Nappi, D. Riccio, and H. Wechsler, "Mobile iris challenge evaluation (MICHE)-I, biometric iris dataset and protocols," *Pattern Recognit. Lett.*, vol. 57, pp. 17–23, May 2015.
- [32] H. Hofbauer, F. Alonso-Fernandez, P. Wild, J. Bigun, and A. Uhl, "A ground truth for iris segmentation," in *Proc. 22nd Int. Conf. Pattern Recognit.*, Stockholm, Sweden, 2014, pp. 527–532.
- [33] R. R. Jillela and A. Ross, "Segmenting iris images in the visible spectrum with applications in mobile biometrics," *Pattern Recognit. Lett.*, vol. 57, pp. 4–16, May 2015.
- [34] S. Thavalengal, P. Bigioi, and P. Corcoran, "Iris authentication in handheld devices—Considerations for constraint-free acquisition," *IEEE Trans. Consum. Electron.*, vol. 61, no. 2, pp. 245–253, May 2015.
- [35] N. Paragios and R. Deriche, "Geodesic active contours and level sets for the detection and tracking of moving objects," *IEEE Trans. Pattern Anal. Mach. Intell.*, vol. 22, no. 3, pp. 266–280, Mar. 2000.
- [36] W.-P. Choi, K.-M. Lam, and W.-C. Siu, "An adaptive active contour model for highly irregular boundaries," *Pattern Recognit.*, vol. 34, no. 2, pp. 323–331, Feb. 2001.
- [37] M. A. M. Abdullah, S. S. Dlay, and W. L. Woo, "Fast and accurate pupil isolation based on morphology and active contour," in *Proc. 4th Int. Conf. Signal Image Process. Appl. (ICSIT)*, Nottingham, U.K., 2014, pp. 418–420.
- [38] D. Comaniciu and P. Meer, "Mean shift: A robust approach toward feature space analysis," *IEEE Trans. Pattern Anal. Mach. Intell.*, vol. 24, no. 5, pp. 603–619, May 2002.
- [39] N. Otsu, "A threshold selection method from gray-level histograms," *IEEE Trans. Syst., Man, Cybern.*, vol. 9, no. 1, pp. 62–66, Jan. 1979.
- [40] H. Proenca, "Iris recognition: On the segmentation of degraded images acquired in the visible wavelength," *IEEE Trans. Pattern Anal. Mach. Intell.*, vol. 32, no. 8, pp. 1502–1516, Aug. 2010.
- [41] L. Sigal, S. Sclaroff, and V. Athitsos, "Skin color-based video segmentation under time-varying illumination," *IEEE Trans. Pattern Anal. Mach. Intell.*, vol. 26, no. 7, pp. 862–877, Jul. 2004.
- [42] C. O. Conaire, N. E. O'Connor, and A. F. Smeaton, "Detector adaptation by maximising agreement between independent data sources," in *Proc. IEEE Conf. Comput. Vis. Pattern Recognit.*, Minneapolis, MN, USA, 2007, pp. 1–6.
- [43] P. Li, X. Liu, L. Xiao, and Q. Song, "Robust and accurate iris segmentation in very noisy iris images," *Image Vis. Comput.*, vol. 28, no. 2, pp. 246–253, 2010.
- [44] E. M. Arvacheh, "A study of segmentation and normalization for iris recognition systems," M.S. thesis, Dept. Syst. Design Eng., Univ. Waterloo, Waterloo, ON, Canada, 2006.
- [45] R. Chen, X. R. Lin, and T. H. Ding, "Iris segmentation for non-cooperative recognition systems," *IET Image Process.*, vol. 5, no. 5, pp. 448–456, Aug. 2011.
- [46] Chinese Academy of Sciences Institute of Automation. *CASIA Iris Image Database*. Accessed on Feb. 2016. [Online]. Available: <http://biometrics.idealtest.org/dbDetailForUser.do?id=4>
- [47] Multimedia University. (2010). *Multimedia University Version 2 Iris Database*. [Online]. Available: <http://pesona.mmu.edu.my/~ctceo/>
- [48] H. Proenca and L. A. Alexandre, "UBIRIS: A noisy iris image database," in *Proc. 13th Int. Conf. Image Anal. Process. (ICIAP)*, Cagliari, Italy, 2005, pp. 970–977.
- [49] H. Proenca and L. A. Alexandre, "The NICE.I: Noisy iris challenge evaluation—Part I," in *Proc. 1st IEEE Int. Conf. Biometr. Theory Appl. Syst.*, Crystal, VA, USA, 2007, pp. 1–4.
- [50] M. A. Luengo-Oroz, E. Faure, and J. Angulo, "Robust iris segmentation on uncalibrated noisy images using mathematical morphology," *Image Vis. Comput.*, vol. 28, no. 2, pp. 278–284, 2010.
- [51] Y. Chen *et al.*, "A highly accurate and computationally efficient approach for unconstrained iris segmentation," *Image Vis. Comput.*, vol. 28, no. 2, pp. 261–269, 2010.
- [52] R. D. Labati and F. Scotti, "Noisy iris segmentation with boundary regularization and reflections removal," *Image Vis. Comput.*, vol. 28, no. 2, pp. 270–277, 2010.
- [53] C.-W. Tan and A. Kumar, "Unified framework for automated iris segmentation using distantly acquired face images," *IEEE Trans. Image Process.*, vol. 21, no. 9, pp. 4068–4079, Sep. 2012.
- [54] T. F. Chan and L. A. Vese, "Active contours without edges," *IEEE Trans. Image Process.*, vol. 10, no. 2, pp. 266–277, Feb. 2001.
- [55] M. A. M. Abdullah, S. S. Dlay, and W. L. Woo, "Fast and accurate method for complete iris segmentation with active contour and morphology," in *Proc. IEEE Int. Conf. Imag. Syst. Tech. (IST)*, 2014, pp. 123–128.
- [56] M. Nabti and A. Bouridane, "New active contours approach and phase wavelet maxima to improve iris recognition system," in *Proc. 4th Eur. Workshop Vis. Inf. Process. (EUVIP)*, Paris, France, 2013, pp. 238–244.
- [57] C.-W. Tan and A. Kumar, "Towards online iris and periocular recognition under relaxed imaging constraints," *IEEE Trans. Image Process.*, vol. 22, no. 10, pp. 3751–3765, Oct. 2013.



Mohammed A. M. Abdullah (M'10) received the B.Sc. and M.Sc. degrees in computer engineering from the University of Mosul, Mosul, Iraq, in 2008 and 2010, respectively. He is currently pursuing the Ph.D. degree with the School of Electrical and Electronic Engineering, Newcastle University, Newcastle upon Tyne, U.K.

He was a Research Assistant with the Department of Electrical Engineering and Electronics, University of Liverpool, Liverpool, U.K., in 2010. His current research interests include pattern recognition and image processing with emphasis on iris recognition.

Mr. Abdullah is a member of British Machine Vision Association and a Student Member of IET.



Wai L. Woo (M'09–SM'11) received the B.Eng. degree (First Class Hons.) in electrical and electronics engineering and the Ph.D. degree in statistical signal processing from Newcastle University, Newcastle upon Tyne, U.K., in 1993 and 1998, respectively.

He is currently a Senior Lecturer with the School of Electrical and Electronic Engineering, Newcastle University. He is also the Director of Operations with the International Branch of Newcastle University, Singapore. His current research interests include mathematical theory and algorithms for nonlinear signal and image processing, machine learning for signal processing, blind source separation, multidimensional signal processing, and signal/image deconvolution and restoration. He has published over 250 papers on the above topics on various journals and international conference proceedings.

Dr. Woo currently serves on the editorial board of several international signal processing journals. He is a Senior Member of IET.



Satnam S. Dlay (M'15) received the B.Sc. degree (Hons.) in electrical and electronic engineering and the Ph.D. degree in very large-scale integration design from Newcastle University, Newcastle upon Tyne, U.K., in 1979 and 1984, respectively.

In recognition of his major achievements, he was appointed as the Personal Chair of Signal Processing Analysis in 2006. He has authored over 250 research papers ranging from biometrics and security, biomedical signal processing, and implementation of signal processing architectures.

Prof. Dlay serves on several editorial boards and has played an active role in numerous international conferences in terms of serving on technical and advisory committees as well as organizing special sessions.



Jonathon A. Chambers (S'83–M'90–SM'98–F'11) received the Ph.D. and D.Sc. degrees in signal processing from the Imperial College of Science, Technology and Medicine (Imperial College London), London, U.K., in 1990 and 2014, respectively.

He is currently the Head of the Communications, Sensors, Signal and Information Processing Group, School of Electrical and Electronic Engineering, Newcastle University, Newcastle upon Tyne, U.K. He has published over 400 conference and journal articles, many of which are in the IEEE journals.

Prof. Chambers has served as an Associate Editor for the IEEE TRANSACTIONS ON SIGNAL PROCESSING from 1997 to 1999 and 2004 to 2007, and a Senior Area Editor from 2011 to 2015. He is a Fellow of the Royal Academy of Engineering, U.K.